Future 3D Additive Manufacturing
The 3DMM2O Conference

# 3D Nano- and Micro-Manufacturing:

# Technology and Technical Application

**REGISTER NOW!**

April 3 – 8, 2022 I Schöntal Monastery, Germany

ADVANCED ELECTRONIC MATERIALS
www.advelectronicmat.de

# Humidity-Induced Nanoscale Restructuring in PEDOT:PSS and Cellulose Nanofibrils Reinforced Biobased Organic Electronics

*Calvin J. Brett,* Ola K. Forslund, Elisabetta Nocerino, Lucas P. Kreuzer, Tobias Widmann, Lionel Porcar, Norifumi L. Yamada, Nami Matsubara, Martin Månsson, Peter Müller-Buschbaum, L. Daniel Söderberg,* and Stephan V. Roth**

**In times where research focuses on the use of organic polymers as a base for complex organic electronic applications and improving device efficiencies, degradation is still less intensively addressed in fundamental studies. Hence, advanced neutron scattering methods are applied to investigate a model system for organic electronics composed of the widely used conductive polymer blend poly(3,4-ethylenedioxythiophene):poly(styrenesulfonate) (PEDOT:PSS) together with nanocellulose as flexible reinforcing template material. In particular, the impact of relative humidity (RH) on the nanostructure evolution is studied in detail. The implications are discussed from a device performance point of view and the changing nanostructure is correlated with macroscale physical properties such as conductivity. The first humidification (95% RH) leads to an irreversible decrease of conductivity. After the first humidification cycle, however, the conductivity can be reversibly regained when returning to low humidity values (5% RH), which is important for device manufacturing. This finding can directly contribute to an improved usability of emerging organic electronics in daily live.**

## 1. Introduction

Organic electronics are rapidly advancing in several fields such as solar cells, batteries and sensors.[1–3] The research is however mostly discussed on their initial device performance, whereas long-term effects due to restructuring on the nanoscale as a result of environmental impacts are rarely addressed. Device degradation can have multiple origins for example due to humidity and surrounding oxygen molecules, which both could change the mesoscale morphology or alter (e.g., oxidize) the chemistry of the materials in use. Additionally, sunlight or electrical cycling can alter devices based on organic polymers.[4]

Poly(3,4-ethylenedioxythiophene):poly (styrenesulfonate) (PEDOT:PSS) as widely used water-soluble conductive polymer

Dr. C. J. Brett, Dr. L. D. Söderberg
Department of Engineering Mechanics
Royal Institute of Technology KTH
Osquars Backe 18, Stockholm 100 44, Sweden
E-mail: calvinbr@kth.se; dansod@kth.se

Dr. C. J. Brett, Dr. L. D. Söderberg
Wallenberg Wood Science Center
Royal Institute of Technology KTH
Teknikringen 52-56, Stockholm 100 44, Sweden

Dr. C. J. Brett, Prof. S. V. Roth
Deutsches Elektronen Synchrotron
Notkestraße 85
22607 Hamburg, Germany
E-mail: stephan.roth@desy.de

The ORCID identification number(s) for the author(s) of this article can be found under https://doi.org/10.1002/aelm.202100137.



**DOI: 10.1002/aelm.202100137**

O. K. Forslund, E. Nocerino, Dr. N. Matsubara, Prof. M. Månsson
Department of Applied Physics
KTH Royal Institute of Technology
Hannes Alfvéns väg 12, Stockholm 114 19, Sweden

L. P. Kreuzer, T. Widmann, Prof. P. Müller-Buschbaum
Lehrstuhl für Funktionelle Materialien
Physik-Department
Technische Universität München
James-Franck-Str. 1, 85748 Garching, Germany

Dr. L. Porcar
Institut Laue-Langevin
71 Avenue des Martyrs, Grenoble 38042, France

Prof. N. L. Yamada
Institute of Materials Structure Science
High Energy Accelerator Research Organization (KEK)
203-1 Shirakata, Tokai
Naka 319-1106, Japan

Prof. P. Müller-Buschbaum
Heinz Maier-Leibnitz Zentrum (MLZ)
Technische Universität München, Lichtenbergstr. 1
85748 Garching, Germany

Prof. S. V. Roth
Fibre and Polymertechnology
Royal Institute of Technology KTH
Teknikringen 52-56, 100 44 Stockholm, Sweden

blend is a model system to study the impact of environmental effects such as humidity. For example, pure and differently doped PEDOT:PSS electrodes were recently studied with neutron reflectometry and a humidity induced swelling of the PEDOT:PSS films was observed.[5–7] The massive swelling of the organic electrodes can significantly affect related devices in applications.

To prevent a considerable swelling and potential destruction of devices based on water-soluble polymers, one can use nanofibers for enhancing the mechanical integrity. In this context, cellulose nanofibrils (CNFs) are gaining more attention as a substitute for glass or carbon fibers due to their particular mechanical properties in combination with sustainable resources and biodegradability.[8] In detail, nanocellulose extracted from wood was shown to be a good reinforcing agent in polymer nanocomposites, while retaining flexibility, lightweight, and mechanical stiffness.[9,10] Chemical functionalization of nanocellulose can be used to further tailor barrier performance of films which might be of crucial benefit for considering nanocellulose as a template for organic electronics.[11]

Conjugated polymers in combination with fibers in thin films or direct fiber applications are extensively studied over the last decade.[12,13] PEDOT:PSS/wood, specifically CNF composites, were widely studied, within applied science, used in electrochemical circuits, mixed ionic-electronic conductors, conductive aerogels as electrodes or paper-based conductive microfluidics to name a few examples.[14–17] Similar conductive polymer nanocomposite aerogels such as poly(3,4-ethylenedioxythiophene)-tosylate (PEDOT:TOS)/CNF showed similar electrical properties, which further supports the fact that CNF is a promising host matrix.[18] In addition, nanocellulose-based aerogels in combination with conductive nanoparticles, such as carbon nanotubes were used as substrates, e.g., for supercapacitors.[19–21]

Scalable deposition techniques need to be considered for a full-scale device manufacturing. Lab-scale techniques such as spin-coating and drop-casting yield well-defined structures, however, they lack the possibility for upscaling. Dip-coating and spray deposition on the other hand are fully scalable with no change in deposition parameters and resulting structural properties compared to the lab scale, which renders both to be industrially relevant.[22] For example, spray deposited PEDOT:PSS and CNF were used to produce large and flexible biobased super capacitors.[1]

X-ray and neutron scattering techniques are suited methods to follow dynamic processes in-situ and have successfully resolved the nanoscale re-assembly of CNF-based 3D objects as well as in thin films during wet and drying conditions.[23] [24,25] Grazing incidence X-ray scattering was used to study and model the organization of PEDOT:PSS on individual CNFs.[26] In fact, GISAXS was used on samples prepared by spray deposition to study the structural changes of nanoparticles during thermal annealing.[27] Time-of-flight neutron reflectometry (TOF-NR) was previously used to study diffusion processes of fullerene derivates into narrow optical band gap polymers.[28]

In the present work, we study the impact of $D_2O$ humidity for contrast enhancement on CNF-reinforced PEDOT:PSS model electrode thin films using grazing incidence small-angle neutron scattering (GISANS) and TOF-NR. We correlate the structural morphology changes during humidity cycles to the electrical performance. The dynamical water contact angle of the nanocomposite is studied to extract the time dependency of water penetration in the thin film. Resolving the morphology, conductivity and water penetration on a highly water affected material allows for future improvements on a nano length scale.

## 2. Results and Discussion

### 2.1. Conductivity

The sheet resistance, resistivity and the conductivity are measured during two full humidity cycles (5 RH% increase to 95 RH%), see **Figure 1a**. The initial conductivity is $\sigma_{1,0}$ = (258.9 ± 0.5) kS m$^{-1}$, decreases to $\sigma_{1,1}$ = (225.3 ± 2.8) kS m$^{-1}$ at high humidity and returns to $\sigma_{2,0}$ = (235.9 ± 0.6) kS m$^{-1}$ when dried. In the second cycle, the conductivity decreases to a similar value as in the first cycle to $\sigma_{2,1}$ = (226.7 ± 1.8) kS m$^{-1}$ and relaxes back to $\sigma_{3,0}$ = (234.4 ± 0.3) kS m$^{-1}$. In the hundreds cycle the conductivity when dry is $\sigma_{100,0}$ = (236.7 ± 0.6) kS m$^{-1}$ and $\sigma_{100,1}$ = (228.2 ± 1.7) kS m$^{-1}$ when wet. Thus, the conductivity decreases to ≈87% ($\sigma_{1,1}/\sigma_{1,0}$) of the initial conductivity during the first humidity cycle and retrieves only 91% ($\sigma_{2,0}/\sigma_{1,0}$) of its initial conductivity back. Further cycles are constant and after 100 cycles the conductivity is still 91% ($\sigma_{100,0}/\sigma_{1,0}$) of the initial conductivity. However, the conductivity cycles after the first one change in a reproducible manner, i.e., $\sigma_{n,m}/\sigma_{n,m}$ = constant for $n, m > 1,1$. Nevertheless, this initial loss is crucial in case applications depend highly on stable electrodes for operability.[1,5] The loss in initial conductivity needs further structural evaluation to understand feasible pre-condition parameters to overcome these issues in organic electronic applications. The aim is to understand the first cycles as these have also usually the strongest influence in organic electronic devices.[29,30]

### 2.2. Nanoscale Morphology

#### *2.2.1. Lateral Restructuring*

The large-scale spray deposited thin films are mounted in a custom-made humidity chamber and dried (5 RH%) prior to the initial GISANS measurement, see Figure S1 in the Supporting Information. The humidity cycling is performed as shown in Figure S1c in the Supporting Information using $D_2O$ to enhance scattering contrast. From each humidity step, two GISANS scattering patterns are recorded and summed up for improved statistics. They are presented according to their respective humidity in **Figure 2** and integrated for further analysis as shown in Figure S2 in the Supporting Information. The scattering patterns show the 2D scattering of the thin film during the humidity cycling. The Yoneda region increases in intensity upon a humidified vapor atmosphere due to swelling and increases in contrast due to $D_2O$ enrichment in the film. Previous own work showed the cyclic changes from cylindrical to spherical appearance in CNF thin films for the first cycle, so 5 RH% to 95 RH%.[25] This initial experiment was extended

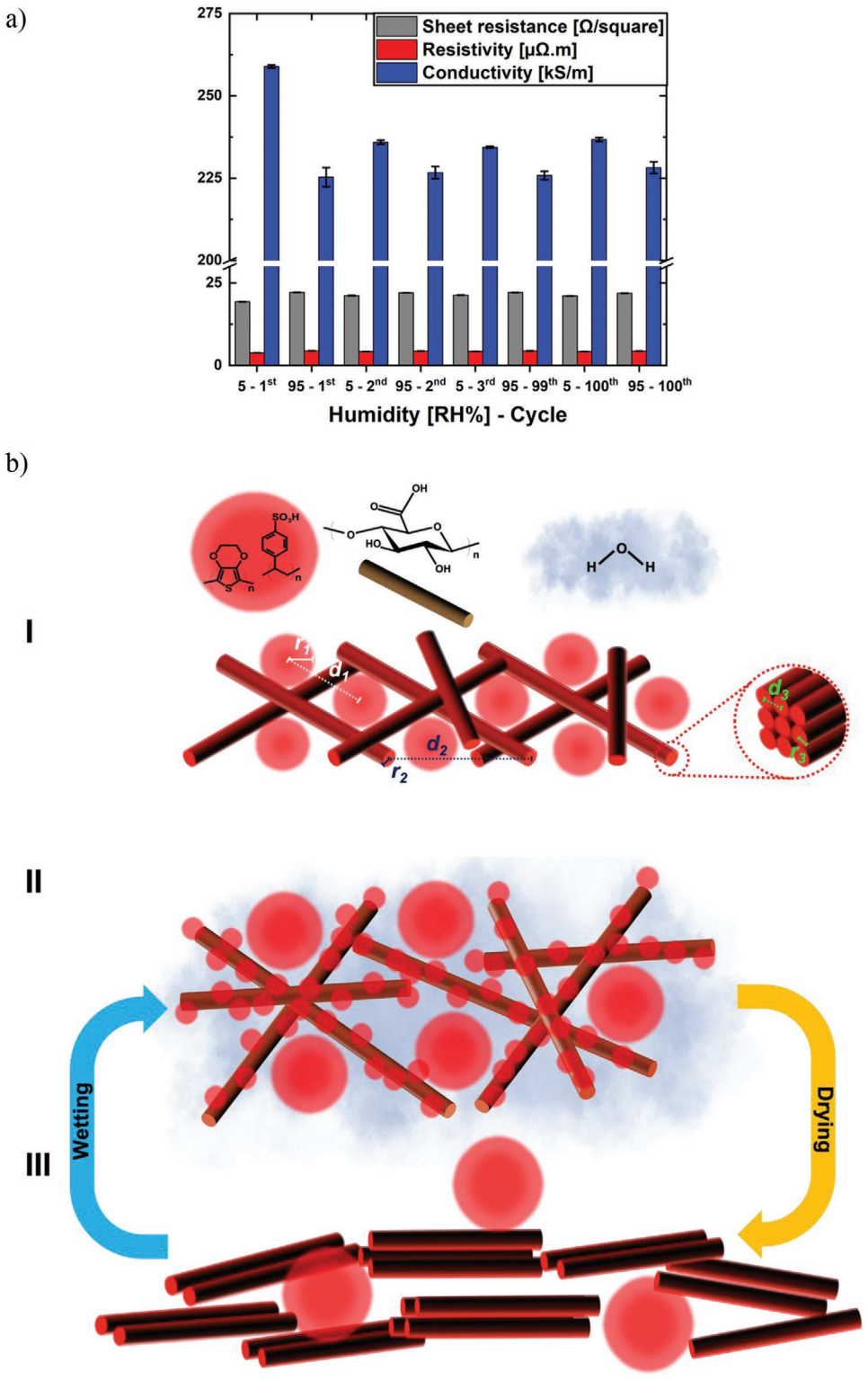


**Figure 1.** Conductivity measurements and schematic of the CNF/PEDOT:PSS nanocomposite during humidity cycling: a) Sheet resistance (grey), resistivity (red), and conductivity (blue) obtained from four-probe measurements on the PEDOT:PSS/CNF thin film. b) Schematic representation of the CNF agglomerates (rods)/PEDOT:PSS (red coating and spherical appearance) network behavior under humidity (blue): I) as deposited dry, II) humid phase, swollen, polymer dewets and distance and radius increase and conductivity decrease, III) dry phase, network collapse distance and radius of polymer increase further and conductivity relaxes. Phase II and III are cyclic repetitive, where the blue arrow marks applied humidity and the yellow arrow the drying.

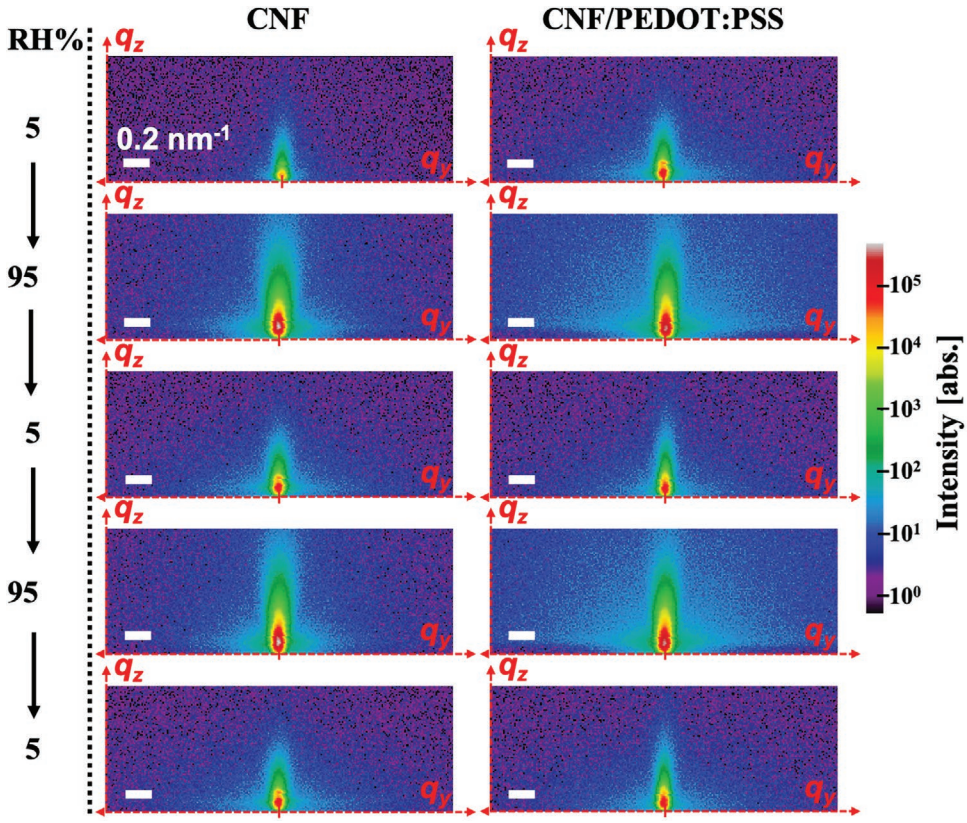


**Figure 2.** 2D GISANS data of the bare CNF template (left) and the CNF/PEDOT:PSS nanocomposite film (right) shown for the five measurements states: Cycling of the humidity from 5 RH% to 95 RH% and back in a repetitive manner.

with this sample set to show the cycling for more cycles, which confirms our previous assumptions for a fully reversible cycling process on pure CNF thin films.[25] We still observe that the largest feature size changes from dry to wet state from a cylindrical to spherical form factor with full reversibility, see Figures 1b and 3c. All fit results are presented in Tables S1 and S2 in the Supporting Information. For the PEDOT:PSS/CNF nanocomposite thin films, we apply the same model as in our initial study (cf. Figure 3a).[25] This model has been widely used, e.g., to study in situ and during *operando* conditions the degradation in organic photovoltaics or thermal degradation of latex nanoparticles using GISAXS.[27,31,32] Furthermore, in a previous publication we correlated that both GISAXS real space microscopy methods as AFM show the same features, which allows us to extract reliable and statistically relevant features by using the above-mentioned model.[25] We are hence confident that the results and the model are relevant. Furthermore, we assume no interference between the different structures and even include the distorted wave Born approximation (DWBA) in a non-resolved way (near $q_y = 0$ nm$^{-1}$) in the model. We find that the two largest features increase in size due to adding the conductive polymer to the CNF network. Yet, this does not induce a shape change: The dry nanocomposite shows cylindrical features and changes its largest feature to a spherical appearance when humidified in the first cycle. We observe reversible shape changes only after the initial restructuring from a cylindrical to a spherical appearance, see Figure 3a,b ("5-2nd"). Hence, the change of the morphology follows the same trend as the conductivity, see Figure 1.

The schematic in Figure 1b presents a model of the restructuring of the composite film. The initial as-deposited film shows PEDOT:PSS covered CNF bundles as well as individual CNFs coated with the polymer blend following the findings of Belaineh et al.[26] When humidified, the polymer partially dewets the CNFs and the CNF bundles. The conductivity decreases at the same time as the film swells and the CNF bundles' distances increase. Upon drying, the film self-assembles to an equilibrium state, in which more of the PEDOT:PSS coated CNFs align in way that promotes conductivity (see Figure 1bIII). In the pure CNF film, the radius of the medium sized cylinders is $r_{2,\mathrm{CNF}} = (8.5 \pm 1.4)$ nm with a center-to-center distance of $d_{2,\mathrm{CNF}} = (75 \pm 9)$ nm. The smallest structures, which can be found in both sample systems, are completely unaffected by the addition of PEDOT:PSS. They have a cylindrical appearance and a radius of $r_{3,\mathrm{CNF}} = (2.5 \pm 0.3)$ nm with a center-to-center distance of $d_{3,\mathrm{CNF}} = (8 \pm 1.7)$ nm. Thus, this smallest structure is in the size region of the individual CNF.[11,24,25,33–36] Previously, we speculated that the largest structure might be pores within the thin film, which can be filled with polymers as shown here. From the model fits we find that the PEDOT:PSS not only affects the largest features; but also the medium sized features (CNF bundles) which increase in size from $r_{2,\mathrm{CNF}} = (8.5 \pm 1.4)$ nm in CNF films to $r_{2,\mathrm{PEDOT:PSS/CNF}} = (11.5 \pm 1.9)$ nm in the composite film. However, the center-to-center distance is

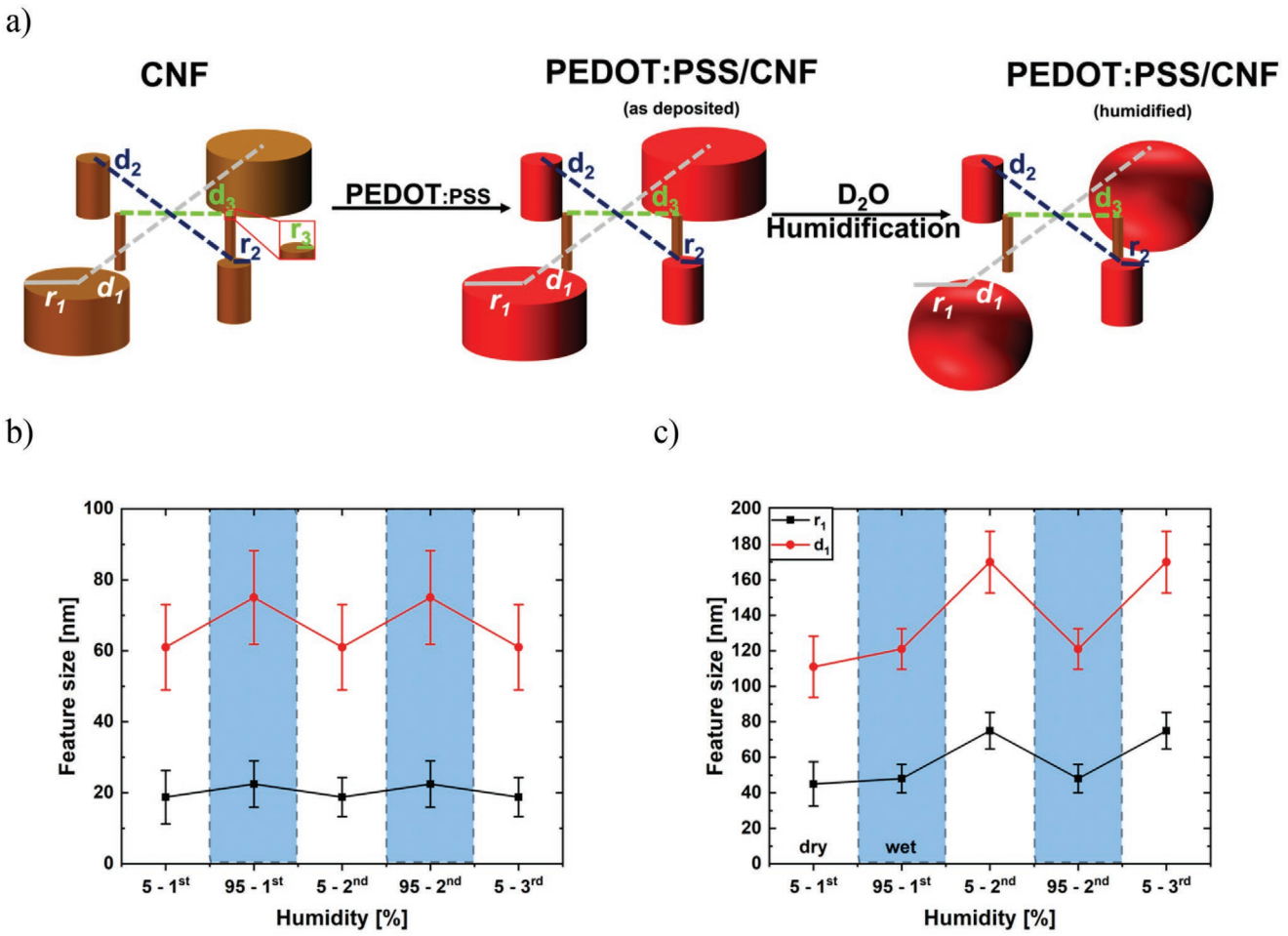


**Figure 3.** a) GISANS model as adapted from Brett et al.,[25] which shows the PEDOT:PSS features (red). During the first humidification step the largest cylindrical structures change to spherical structures. Following cycles show only spherical structures for the PEDOT:PSS/CNF nanocomposite. The CNF thin film shows a fully reversible cylindrical to spherical transformation in dry and wet environment, respectively. Characteristic structures determined in the fits for b) pure CNF and c) PEDOT:PSS/CNF, respectively.

not affected by this $d_{2,\mathrm{CNF}} \approx d_{2,\mathrm{PEDOT:PSS/CNF}} = (73 \pm 11.7)$ nm. Similar sizes of PEDOT and PSS on CNF were reported earlier by Belaineh et al. and also observed through molecular dynamics simulations performed by Mehandzhiyski and Zozoulenko, confirming these findings.[26,37] The largest structure is presented in Figure 3b. It experiences an initial change from a cylindrical to a spherical appearance before cyclic size effects in combination with a swelling process occur ("5-2nd").

### 2.2.2. Swelling

TOF-NR measurements are performed on the same sample system with thinner films ($\delta \approx$ 20–30 nm) to gain a better understanding on the density gradient and changes during humidity cycling of such complex nanocomposites. The reflectometry data is shown in **Figure 4**a together with fits for all humidity cycles performed on the PEDOT:PSS/CNF nanocomposite. Clear differences are observed: The initial dry film SLD does not overlap with the re-dried film after the first humidity cycle as seen in the GISANS measurements concerning lateral structures. The fits yield also the scattering length density (SLD) profile, which is presented in Figure 4b for all films during the different humidification steps. It depicts a strong density gradient along the surface normal with high roughness. We speculate that this gradient originates from the used spray deposition technique (see for details Tables S3–S5 in the Supporting Information). Spray deposition is a non-equilibrium deposition process under applied heat where droplets evaporate on the position they are deposited.[38] The humidified nanocomposite film is swells only very little compared to previously reported experiments on pure PEDOT:PSS electrodes.[5] Obviously, the film swelling is limited by the mechanical integrity enhancement due to the CNF reinforcing agent.[5] The CNF network is the structural matrix and hence the polymer PEDOT:PSS has to adopt to the contracting lateral space and swells in vertical direction. In the pure PEDOT:PSS and CNF films on the contrary, the expected swelling effects are observed immediately (see Figure S4b,d in the Supporting Information). One can conclude that the changes in the CNF/PEDOT:PSS nanocomposite is dominated by the PEDOT:PSS. The pure CNF thin film shows nearly full reversibility under cyclic humidification.

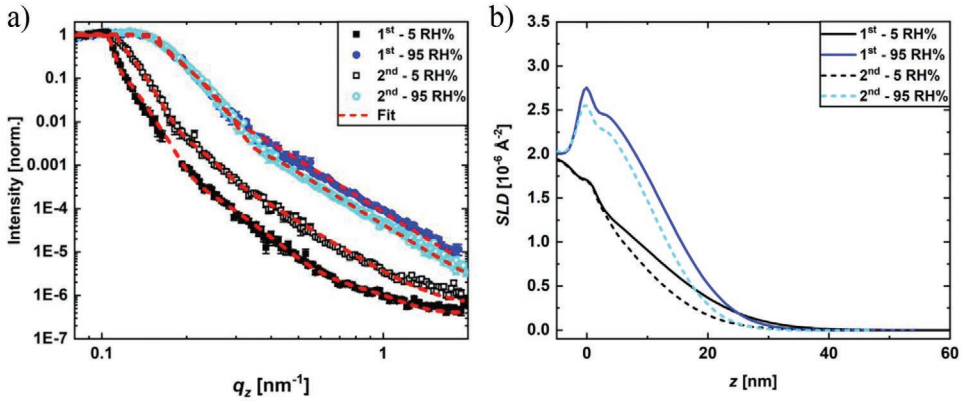


**Figure 4.** a) NR data from the PEDOT:PSS/CNF nanocomposite thin films under humidity cycling is shown together with the corresponding fits (red dashed line). Two full humidity cycles are performed starting at 5 RH% (black) and humidifying till 95 RH% (1st blue, 2nd cyan), the first cycle is marked with closed symbols and the second cycle with open symbols. b) SLD profiles plotted versus the sample thickness *z*. The black lines mark the dry (5 RH%) and the blue (1st) and cyan (2nd) the wet (95 RH%), the full lines show the first and the dashed lines the second cycle. For details see Table S3 in the Supporting Information.

Although, after the first cycle the thickness of the film as well as the density gradient slightly decrease, which can be attributed to equilibration of the water-soluble polymers due to rewetting. On all studied films, we observe that the water ($D_2O$) is penetrating the full film and accumulating at the substrate interface during the humidification (see peak in Figure 4 and Figure S4 (Supporting Information) around $z = 0$ nm). Only the CNF film shows that the water accumulates not only at the substrate interface but also at the CNF/air interface (see Figure S4a,c in the Supporting Information (peak at $z \approx 40$ nm) and Table S5 in the Supporting Information).

### 2.3. Surface Wetting

Full characterization of dynamic water contact angle measurements are performed to study the effect of water droplets on the surface of the PEDOT:PSS/CNF nanocomposite. The dynamic contact angle measurements are performed for 3 min and showed that the contact angle on a pure CNF thin film does not vary and is nearly constant over time (see **Figure 5** and Table S6 (Supporting Information)). The pure PEDOT:PSS and the PEDOT:PSS/CNF nanocomposite show a double exponential decay of the water contact angle. Comparing the pure PEDOT:PSS and the nanocomposite, one observes that the initial contact angle is decreased by ≈3° for the nanocomposite. The first exponential component has a time variable of $t_1$ (composite) ≈12 s and $t_1$ (PEDOT:PSS) ≈14 s for the PEDOT:PSS/CNF nanocomposite and the pure PEDOT:PSS thin film, respectively. This time might be attributed to the time it takes for the water to permeate the thin film and swell it. PEDOT:PSS, which fills the voids (largest structures $r_1$) in the CNF matrix is water soluble and thus promotes water imbibition. In the NR data, we observe that CNF stabilizes the thin film as the film does not swell as expected and the initial film thickness remains unchanged. From dynamic water contact angle measurements, one can conclude a better processing with water by the addition of CNFs to PEDOT:PSS. The induced CNFs increase the water attraction of the thin film, which is favorable for water-based functionalization.

## 3. Conclusion

The impact of humidity vapor and water droplets on an organic electronic model system based on PEDOT:PSS and CNF is studied. We elucidate the impact from the water vapor and water droplets on the nanoscale morphology and the wettability as well as the conductivity. We find that the initial conductivity decreases in a humid environment to 87% of its initial value. The recovery of the conductivity upon full drying is also affected by the humidification and only 91% of the initial conductivity can be retrieved. Further humidity cycling shows on the other hand that the change in conductivity becomes stagnant.

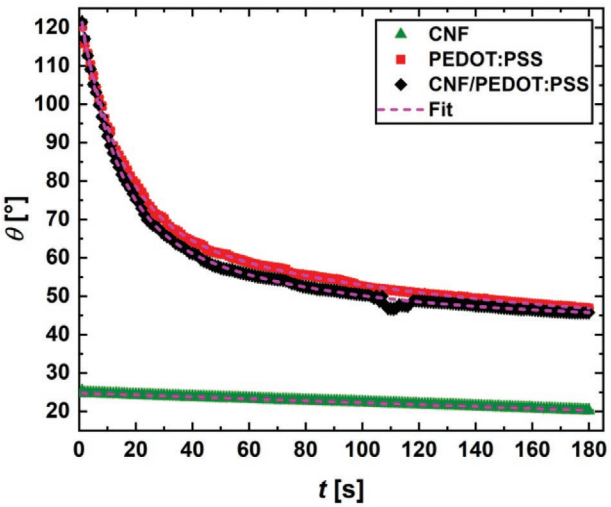


**Figure 5.** Dynamic water contact angle measurements performed on the bare CNF (green) and PEDOT:PSS (red) films as well as on the nanocomposite CNF/PEDOT:PSS (black). The measurements were performed over a timescale of 180 s and each second the contact angle was measured and subsequently fitted using a linear (CNF) or a double exponential decay (PEDOT:PSS based films). At around 110 s at CNF/PEDOT:PSS sample experimental noise is diverging the measured contact angles due to automated refocusing of the microscope at that time. For details see Table S6 in the Supporting Information.

In the first humidification cycle, we observe a non-reversible change in the nanoscale structure from a cylindrical appearance to a spherical appearance, which can be interpreted as a change in the size of the voids. A second humidification cycle shows changes in sizes, but these changes are fully reversible and cause no further irreversible changes in the conductivity. NR data confirm the reinforcing capabilities of nanocellulose from the reduced film swelling. Dynamic water contact angle measurements show that the use of CNFs as reinforcing agent increases the hydrophilicity of the composite, which becomes important for subsequent water-based processing steps.

Thus, this study reveals that the use of CNF can improve the stability of PEDOT:PSS electrodes for the use in organic electronics under a changing humid environment. Besides limiting the working ranges to specific humidity levels, a pre-conditioning of the nanocomposite electrodes appears as a promising alternative. Pre-humidified nanocomposited PEDOT:PSS/CNF electrodes offer a pathway to devices in which the structures have undergone the initial large changes already and are stable with respect to nanostructure and conductivity in the device application. Similar pre-conditioning approaches are very successfully used in other energy materials such as for example lithium ion batteries and can offer the needed breakthrough for green organic electronics.

## 4. Experimental Section

*Material*: Silicon wafers (one-side polished, boron-doped, 1–30 Ω.cm, (100), Si-Mat, Germany) were cut in (100 × 20) $mm^2$ size and cleaned in an acetone ultrasonic bath for 15 min. Subsequently, the wafers were flushed with acetone (>97%), 2-propanol (98%), ethanol (96%, all Sigma-Aldrich, Germany), and ultrapure water (18.2 MΩ cm, Milli-Q, Merck KGaA, Germany). After organic traces removal, the wafers were cleaned in an acid bath for 15 min at 80 °C under continues stirring of the cleaning bath. The bath was based on ultrapure water (37.5 mL), sulphuric acid (190 mL, 96%, Sigma-Aldrich) and hydrogen peroxide (87.5 mL, 30%, VWR International LLC., USA). Next, the samples were flushed with ultrapure water and kept in a sealed ultrapure water container until usage. Prior to spray deposition, the wafers were blown dry using nitrogen.

CNF were prepared from bleached wood fibers (40% scots pine and 60% Norwegian spruce) followed by the TEMPO-mediated oxidation (2,2,6,6-tetramethylpiperidinyl-1-oxyl) procedure introduced by Isogai et al. and the same batch was used as in previous publications.[25,39] The CNF surface charge was 1000 µmol $g^{-1}$. CNF with a surface charge of 1000 µmol $g^{-1}$ were chosen due to the low contact angle of water expecting a good imbibition of the water-based PEDOT:PSS in the CNF matrix.[25] The mean length was around 538 nm which was previously shown by Geng et al. and can be follows the trend the higher the charge the shorter the CNFs.[40] The resulting CNF gel was further diluted using $D_2O$ (99.9%, Merck KGaA, Germany) to 0.07 wt% and further processed by mixing and centrifuging in three steps. This allowed for protonating the CNF via mechanical mixing at 10 000 rpm for 10 min (UltraTurrax, IKA, Germany), ultrasonic generator (30% amplitude, 10 min, Sonics, Vibra-Cell CV33, USA) and then centrifuged at 4000 rpm for 60 min (MegaStar 3.0, VWR International LLC., USA). The resulting suspension was used for spray deposition.

PEDOT:PSS (poly(3,4-ethylenedioxythiophene):poly(styrenesulfonate), 1.1% in $H_2O$, surfactant-free, Sigma-Aldrich, Belgium) was processed for 15 min in an ultrasonic bath and filtered through a PES-filter (0.45 µm, polyethersulfone, Ossila Ltd., UK) to remove large aggregates prior to spray deposition. For the CNF/PEDOT:PSS nanocomposite samples both dispersions were mixed 1:1 by volume and stirred for 15 min at 5000 rpm using the aforementioned mechanical mixer.

*Spray Deposition*: The sample deposition was done on a laboratory setup consisting of a motorized linear stage, a spray nozzle and a hotplate, which all was controlled using a custom Python program. The hotplate (EMS 1000 series, Electronic Micro Systems, UK) was set to 120 °C during the spray deposition. The motorized linear stage (LTS300/M, Thorlabs Inc., USA) allowed for moving the spray nozzle back and forth above the sample to cover a large area homogeneously during the deposition. The nozzle was moved laterally 130 mm crossing the aforementioned sample with a length of 100 mm by 15 mm on both sides. A speed of 50 mm $s^{-1}$ and an acceleration of 50 mm $s^{-2}$ were used. The spray nozzle (Compact JAU D555000, Spray Systems, Germany) consisted of a siphon-based liquid container (12 mL), a cylinder (gas controlled, 6 bar) to open and close and a gas feeding line (nitrogen, 1 bar). The spray nozzle was kept 200 mm above under normal incidence in regard to the samples surface. The spray protocol for conductivity, water contact angle and GISANS experiments was 100 ms spraying 650 ms waiting and a repetition of this cycle 85 times for CNF and 80 times for PEDOT:PSS. All PEDOT:PSS containing thin films were further annealed after deposition for 15 min at 120 °C. In case of NR, the protocol was adjusted to 10 cycles.

*Conductivity Measurements*: Four-probe conductivity measurements were performed on the humidity cycled samples to correlate structural changes to modifications in sheet resistance and conductivity. The humidification was performed in a glass desiccator with $D_2O$ humidity attached in a flow-controlled nitrogen gas line (EL-FLOW Select, Bronkhorst High-Tech BV, Netherlands). The humidity was measured using a MEAS WV1.1 (WPP1008001, TE Connectivity Sensors, China) The measurements were performed using a Four-point setup T2001A (Ossila Ltd., UK) and the raw data were analyzed using Ossila Sheet Resistance (v2.0.3.3, Ossila Ltd, UK) software. The probes were spring loaded and separated by 1.27 mm, the set target current was 10 mA and the voltage increment was 0.1 V. Sheet resistance measurements were performed 25 times and 2048 samples per point were measured. The sample size for conductivity measurements were (20 × 80) $mm^2$.

*Contact Angle Measurements*: The dynamic water contact angle measurements were conducted using an OCA20 (Data Physics, Germany) contact angle measurement. For checking sample homogeneity on each sample three droplet experiments on different positions were performed, by depositing 5 µL ultrapure water on the surface of the thin film with an automatic syringe pump . In sessile-drop configuration a camera captured every second the droplet on the surface. The time-dependent water contact angle from the left and right of the droplet was measured and averaged using the software SCA20 (Data Physics, Germany).

*Neutron Scattering*: Grazing incidence small-angle neutron scattering (GISANS) experiments were performed at the beamline D22 at ILL in Grenoble, France.[41] A wavelength of $\lambda = 9$Å with $\frac{\Delta\lambda}{\lambda} = 10\%$ was used, a sample-to-detector distance (SDD) of $SDD = 6$ m and a (2 ×10) $mm^2$ aperture to gain a small beam shape on the sample surface. Each sample was aligned on a goniometer and the incidence angle was set to $\alpha_i = 1°$ and integrated for two times 1 h. For humidification a chamber equipped with thin aluminum windows was used to mount the samples and allowed them to tune the humidity between 5 RH% and 95 RH%, see Figure S1 in the Supporting Information. In order to generate a humid atmosphere, nitrogen gas was bubbled through a bottle of $D_2O$ (99.9%, Merck KGaA, Germany) and flow-controlled inserted in the humidity chamber. Before each measurement, the samples were kept 30 min at the desired humidity to establish equilibrium conditions during the measurement. The humidity cycling plot can be seen in Figure S1c in the Supporting Information.

*Neutron Reflectometry*: Time-of-flight neutron reflectometry (TOF-NR) measurements were performed at the BL16/SOFIA reflectometer at J-PARC/MLF in Tokai, Japan.[42,43] Sample preparation was done as before, however, thinner films of ≈20 nm were produced to resolve the Kiessig oscillations. For the NR measurements three incident Θ-angles were

chosen, $\Theta_1 = 0.3°$, $\Theta_2 = 0.75°$, $\Theta_3 = 1.8°$ allowing a mapping of the q-space from $q_z \approx 0.08$ nm$^{-1}$ to $q_z \approx 3.5$ nm$^{-1}$ with a minimum wavelength of $\lambda_{min}$ = 0.2 nm and a resolution of $\Delta q/q$ = 2%. The raw data was retrieved using the software IGOR Pro (v. 6.37) and the SOFIA converter plugin (v. 2.7182). For humidification of the samples a beamline provided chamber was used, which held all samples at the same time and could cycle the samples between 5 RH% and 95 RH%. After each change in humidity the samples were kept at the desired humidity for 30 min to reach equilibrium. All characterization measurements were performed at room temperature.

## Supporting Information

Supporting Information is available from the Wiley Online Library or from the author.

## Acknowledgements

The authors thank Nitesh Mittal for kindly providing the nanocellulose. The authors thank Shun Yu for help during GISANS beamtime. C.J.B. and S.V.R. acknowledge financial support from DESY strategic fund (DSF) "Investigation of processes for spraying and spray-coating of hybrid cellulose-based nanostructures." DESY (Hamburg, Germany) is a member of the Helmholtz Association HGF. This research has been funded by the Knut and Alice Wallenberg Foundation through Wallenberg Wood Science Center at KTH. L.P.K. and T.W. acknowledge the BMBF project "Flexiprobe" (Grant Number 05K16WOA) and P.M.-B. International Research Training Group 2022 Alberta/Technical University of Munich International Graduate School for Environmentally Responsible Functional Hybrid Materials (ATUMS). O.K.F., E.N., and M.M. acknowledge funding from the Swedish Research Council, VR (Dnr. 2016-06955) as well as the Swedish Foundation for Strategic Research (SSF) within the Swedish national graduate school in neutron scattering (SwedNess). TOF-NR experiments were carried out using the SOFIA neutron instrument at the MLF pulsed neutron source at J-PARC in Tokai, Japan (Proposal No. 2019B0293). GISANS experiments were carried out at D22 neutron instrument at ILL neutron reactor source in Grenoble, France (Proposal No. 9-11-1885).

Open access funding enabled and organized by Projekt DEAL.

## Conflict of Interest

The authors declare no conflict of interest.

## Data Availability Statement

The data that support the findings of this study are openly available from Institut Laue-Langevin (ILL) at https://doi.org/10.5291/ILL-DATA.9-11-1885.

## Keywords

cellulose, conductivity, GISANS, humidity effect, neutron reflectivity, organic electronics, PEDOT:PSS, soft matter

Received: March 11, 2021
Published online: May 7, 2021

[1] M. G. Say, R. Brooke, J. Edberg, A. Grimoldi, D. Belaineh, I. Engquist, M. Berggren, *npj Flex. Electron.* **2020**, *4*, 14.
[2] J. Wu, X. Che, H.-C. Hu, H. Xu, B. Li, Y. Liu, J. Li, Y. Ni, X. Zhang, X. Ouyang, *J. Mater. Chem. A* **2020**, *8*, 5442.
[3] J. F. Peters, A. P. Cruz, M. Weil, *Batteries* **2019**, *5*, 10.
[4] W. Wang, C. J. Schaffer, L. Song, V. Körstgens, S. Pröller, E. D. Indari, T. Wang, A. Abdelsamie, S. Bernstorff, P. Müller-Buschbaum, *J. Mater. Chem. A* **2015**, *3*, 8324.
[5] L. Bießmann, L. P. Kreuzer, T. Widmann, N. Hohn, J.-F. Moulin, P. Müller-Buschbaum, *ACS Appl. Mater. Interfaces* **2018**, *10*, 9865.
[6] G. E. Pérez, G. Bernardo, H. Gaspar, J. F. K. Cooper, F. Bastianini, A. J. Parnell, A. D. F. Dunbar, *ACS Appl. Mater. Interfaces* **2019**, *11*, 13803.
[7] J.-P. Veder, K. Patel, M. Sohail, S. P. Jiang, M. James, R. De Marco, *Electroanalysis* **2012**, *24*, 140.
[8] T. Rosén, B. S. Hsiao, L. D. Söderberg, *Adv. Mater.* **2020**, https://doi.org/10.1002/adma.202001238.
[9] X. Xu, F. Liu, L. Jiang, J. Y. Zhu, D. Haagenson, D. P. Wiesenborn, *ACS Appl. Mater. Interfaces* **2013**, *5*, 2999.
[10] N. Mittal, F. Ansari, K. Gowda.V, C. Brouzet, P. Chen, P. T. Larsson, S. V. Roth, F. Lundell, L. Wågberg, N. A. Kotov, L. D. Söderberg, *ACS Nano* **2018**, *12*, 6378.
[11] P. T. Larsson, J. Hellwig, V. López Durán, P. A. Larsson, L. Wågberg, *ACS Appl. Nano Mater.* **2018**, *1*, 1959.
[12] C. Müller, L. Ouyang, A. Lund, K. Moth-Poulsen, M. M. Hamedi, *Adv. Mater.* **2019**, *31*, 1807286.
[13] A. Lund, N. M. van der Velden, N.-K. Persson, M. M. Hamedi, C. Müller, *Mater. Sci. Eng., R* **2018**, *126*, 1.
[14] J. Edberg, A. Malti, H. Granberg, M. M. Hamedi, X. Crispin, I. Engquist, M. Berggren, *Flexible Printed Electron.* **2017**, *2*, 045010.
[15] A. Malti, J. Edberg, H. Granberg, Z. U. Khan, J. W. Andreasen, X. Liu, D. Zhao, H. Zhang, Y. Yao, J. W. Brill, I. Engquist, M. Fahlman, L. Wågberg, X. Crispin, M. Berggren, *Adv. Sci.* **2016**, *3*, 1500305.
[16] J. Garemark, X. Yang, X. Sheng, O. Cheung, L. Sun, L. A. Berglund, Y. Li, *ACS Nano* **2020**, *14*, 7111.
[17] M. M. Hamedi, A. Ainla, F. Güder, D. C. Christodouleas, M. T. Fernández-Abedul, G. M. Whitesides, *Adv. Mater.* **2016**, *28*, 5054.
[18] H. Françon, Z. Wang, A. Marais, K. Mystek, A. Piper, H. Granberg, A. Malti, P. Gatenholm, P. A. Larsson, L. Wågberg, *Adv. Funct. Mater.* **2020**, *30*, 1909383.
[19] G. Nyström, A. Marais, E. Karabulut, L. Wågberg, Y. Cui, M. M. Hamedi, *Nat. Commun.* **2015**, *6*, 7259.
[20] K. Shi, X. Yang, E. D. Cranston, I. Zhitomirsky, *Adv. Funct. Mater.* **2016**, *26*, 6437.
[21] X. Yang, K. Shi, I. Zhitomirsky, E. D. Cranston, *Adv. Mater.* **2015**, *27*, 6104.
[22] J. J. Richardson, M. Bjornmalm, F. Caruso, *Science* **2015**, *348*, aaa2491.
[23] H. Li, M. Kruteva, K. Mystek, M. Dulle, W. Ji, T. Pettersson, L. Wågberg, *ACS Nano* **2020**, *14*, 6774.
[24] W. Ohm, A. Rothkirch, P. Pandit, V. Körstgens, P. Müller-Buschbaum, R. Rojas, S. Yu, C. J. Brett, D. L. Söderberg, S. V. Roth, *J. Coat. Technol. Res.* **2018**, *15*, 759.
[25] C. J. Brett, N. Mittal, W. Ohm, M. Gensch, L. P. Kreuzer, V. Körstgens, M. Månsson, H. Frielinghaus, P. Müller-Buschbaum, L. D. Söderberg, S. V. Roth, *Macromolecules* **2019**, *52*, 4721.
[26] D. Belaineh, J. W. Andreasen, J. Palisaitis, A. Malti, K. Håkansson, L. Wågberg, X. Crispin, I. Engquist, M. Berggren, *ACS Appl. Polym. Mater.* **2019**, *1*, 2342.
[27] J. Engström, C. J. Brett, V. Körstgens, P. Müller-Buschbaum, W. Ohm, E. Malmström, S. V. Roth, *Adv. Funct. Mater.* **2020**, *30*, 1907720.
[28] A. J. Clulow, C. Tao, K. H. Lee, M. Velusamy, J. A. McEwan, P. E. Shaw, N. L. Yamada, M. James, P. L. Burn, I. R. Gentle, P. Meredith, *Langmuir* **2014**, *30*, 11474.
[29] H. Olsson, G. Nyström, M. Strømme, M. Sjödin, L. Nyholm, *Electrochem. Commun.* **2011**, *13*, 869.

[30] L. Nyholm, G. Nyström, A. Mihranyan, M. Strømme, *Adv. Mater.* **2011**, *23*, 3751.
[31] C. J. Schaffer, C. M. Palumbiny, M. A. Niedermeier, C. Jendrzejewski, G. Santoro, S. V. Roth, P. Müller-Buschbaum, *Adv. Mater.* **2013**, *25*, 6760.
[32] Q. Chen, C. J. Brett, A. Chumakov, M. Gensch, M. Schwartzkopf, V. Körstgens, L. D. Söderberg, A. Plech, P. Zhang, P. Müller-Buschbaum, S. V. Roth, *ACS Appl. Nano Mater.* **2021**, *4*, 503.
[33] A. Dufresne, *Mater. Today* **2013**, *16*, 220.
[34] M. Wang, I. V. Anoshkin, A. G. Nasibulin, J. T. Korhonen, J. Seitsonen, J. Pere, E. I. Kauppinen, R. H. A. Ras, O. Ikkala, *Adv. Mater.* **2013**, *25*, 2428.
[35] T. Saito, S. Kimura, Y. Nishiyama, A. Isogai, *Biomacromolecules* **2007**, *8*, 2485.
[36] M. Henriksson, G. Henriksson, L. A. Berglund, T. Lindström, *Eur. Polym. J.* **2007**, *43*, 3434.
[37] A. Y. Mehandzhiyski, I. Zozoulenko, *ACS Appl. Energy Mater.* **2019**, *2*, 3568.
[38] B. Su, H. A. Caller-Guzman, V. Körstgens, Y. Rui, Y. Yao, N. Saxena, G. Santoro, S. V. Roth, P. Müller-Buschbaum, *ACS Appl. Mater. Interfaces* **2017**, *9*, 43724.
[39] A. Isogai, T. Saito, H. Fukuzumi, *Nanoscale* **2011**, *3*, 71.
[40] L. Geng, N. Mittal, C. Zhan, F. Ansari, P. R. Sharma, X. Peng, B. S. Hsiao, L. D. Söderberg, *Macromolecules* **2018**, *51*, 1498.
[41] S. V. Roth, C. J. Brett, L. P. Kreuzer, M. Månsson, P. Müller-Buschbaum, L. Porcar, L. D. Söderberg, T. Widmann, S. Yu, *GISANS Study on Conducting Polymer Infiltration in Porous Cellulose Thin Films*, Institut Laue-Langevin (ILL): Institut Laue-Langevin (ILL), Institut Laue-Langevin (ILL), **2018**, https://doi.org/10.5291/ILL-DATA.9-11-1885.
[42] N. L. Yamada, N. Torikai, K. Mitamura, H. Sagehashi, S. Sato, H. Seto, T. Sugita, S. Goko, M. Furusaka, T. Oda, M. Hino, T. Fujiwara, H. Takahashi, A. Takahara, *Eur. Phys. J. Plus* **2011**, *126*, 108.
[43] K. Mitamura, N. L. Yamada, H. Sagehashi, N. Torikai, H. Arita, M. Terada, M. Kobayashi, S. Sato, H. Seto, S. Goko, M. Furusaka, T. Oda, M. Hino, H. Jinnai, A. Takahara, *Polym. J.* **2013**, *45*, 100.